An analytical formula to identify the parameters of the energy-based hysteresis model

Riccardo Scorretti, Fabien Sixdenier

Version of Record: https://www.sciencedirect.com/science/article/pii/S0304885321009768
Manuscript_9244e15afbb85ae7dbc7a0139c85cf06

An analytical formula to identify the parameters of the energy-based hysteresis model

Riccardo Scorretti*, Fabien Sixdenier

Univ Lyon, Université Claude Bernard Lyon 1, Ecole Centrale de Lyon, INSA Lyon, CNRS, Ampère, Villeurbanne, France

Abstract

Energy-based models (also called Vector Play models) are a class of phenomenological models of magnetic hysteresis. In this work an original identification method is presented. The main advantage of this method is its speed and its robustness. Conversely to optimization-based methods, which are prone to convergence problems, the new method is based on analytical formulas. The method is tested experimentally with three different materials (a ferrite and two non oriented steels), and provide an accuracy comparable to classical identification methods, with a much lower computational cost.

Keywords: Hysteresis, Energy based model, Vector play model

1. Introduction

Accurate modeling of hysteresis is important in order to model[1, 2, 3] and optimize engineering applications[4, 5, 6]. Many phenomenological models of hysteresis have been proposed. The classical Preisach[7] models and its vector extensions like Preisach-Mayergoyz model[8, 9, 10, 11] and the Vector Hysteron model[12, 13, 14, 15, 16] are known to be accurate, but have a very high computational cost. On the other hand, Jiles-Atherton models [17, 18, 19, 20] are much less computationally intensive, but also less accurate in particular with

*Corresponding author
Email addresses: riccardo.scorretti@univ-lyon1.fr (Riccardo Scorretti), fabien.sixdenier@univ-lyon1.fr (Fabien Sixdenier)

complex signals (harmonics, PWM) [21]. The energy-based (EB – also called vector play) models are phenomenological models of static magnetic hysteresis [22] which have many desirable properties. Conversely to other models like the classical Preisach [7] and Jiles-Atherton [17] models, EB models are intrinsically vectorial and provides an accurate energy balance [23]. Both these features are key assets for practical application, like transformer and motor design [24]. Another nice feature of this model is that the number of parameters is not fixed *a priori*, so that it can be adjusted so as to meet requirements on accuracy: this is important because, in view of 3D numerical computations of realistic devices, models should be kept as light as possible.

Like any other model, identification from experimental measurements is a key point. Most of identification methods rely on numerical optimization [25, 23], and are thereby slow and prone to convergence problems, including convergence to suboptimal local minima. A quite different approach is proposed in [26, 27, 28], but here too the identification is taken on numerically by evaluating many times a recursive expression, starting from many different initial points. This procedure ultimately provides a high number of samples of the functional which has to be identified. This functional is then discretized so as to be practically used in computational electromagnetism programs.

In this work we present an original identification method, which has the unique feature to rely on a closed form analytical formula. It is demonstrated that this new identification method is remarkably fast and robust.

The materials and methods are described in the next section. The theory of the method is introduced in the third section. The robustness of the method is demonstrated by using three different materials: a ferrite and two non oriented electrical steels. Moreover, the method is compared with respect of a different identification method [25] in order to compare the computational time and the accuracy of the predictions.

2. Materials and methods

The identification method has been tested with three different materials and various different experimental conditions. This section gives details about these materials and measurements.

2.1. Ferrite 3C90

The first material is a 3C90 ferrite produced by Ferroxube. It is a $MnZn$ ferrite classically used in power electronics applications [28]. The experimental set is composed of 13 centered minor loops that have been used for identification in quasi-static conditions (50 Hz). A more complex signal composed of a fundamental sinusoidal waveform with a third harmonic of excitation field (not part of the data set) has also been measured to test the robustness of the model.

2.2. TEAM32 laminations

Measurement of loops performed on Fe-Si 3.2% wt have been published in [29]. The dataset is composed of several unidirectional symmetrical loops measured by using the usual Epstein frame at 10 Hz, with different orientations with respect of the rolling directions.

First, the model has been identified by using the loops measured along the rolling direction; the loops measured at 90° with respect of the rolling direction were used to assess the predictive capability of the model.

Then the roles of the two measurement sets have been exchanged: the loops measured at 90° have been used for the identification, and the loops measured at 0° have been used to assess the predictive capability.

2.3. Non oriented grains electrical steel

Scalar and vector measurement performed on a non-oriented grain electrical steel have been published in [30] (courtesy of Dr. Antonio Faba) at frequencies below 5 Hz [31]. The dataset is composed of several unidirectional symmetrical loops along different orientations, and a genuine vector measurement performed by exciting the material with a Rotational Single Sheet Tester. Only the uniaxial

measurements along the rolling directions were used for identification. The other measurements were used to assess the predictive capability of the model.

2.4. Quantitative indicators

For all the tested materials we used some quantitative indicators used to evaluate the performances of the identification method. These indicators are defined hereafter:

$$\text{RBMAX} = \frac{\max ||\mathbf{b_{sim}}||}{\max ||\mathbf{b_{meas}}||} \tag{1}$$

$$\text{RPOW} = \frac{\oint \mathbf{h_{sim}} \cdot \mathbf{db_{sim}}}{\oint \mathbf{h_{meas}} \cdot \mathbf{db_{meas}}} \tag{2}$$

$$\text{RERR} = \frac{\sqrt{\frac{1}{T}\int_0^T ||\mathbf{b_{meas}} - \mathbf{b_{sim}}||^2 dt}}{\sqrt{\frac{1}{T}\int_0^T ||\mathbf{b_{meas}}||^2 dt}} \tag{3}$$

$$\text{RHCOE} = \frac{h_{coer}^{(sim)}}{h_{coer}^{(meas)}} \tag{4}$$

$$\text{RBREM} = \frac{b_{rem}^{(sim)}}{b_{rem}^{(meas)}} \tag{5}$$

Index RBMAX is the ratio between simulated and measured $\max ||\mathbf{b}||$. In the case of scalar measurements, the index RHCOE and RBREM are the ratios between coercive magnetic field and remanent flux density respectively. The index RERR is the relative root mean square (rms) error on the flux density signals. The index RPOW is the ratio between the simulated and measured loop areas (image of losses).

In the case of RBMAX, RPOW, RHCOE and RBREM values close to 1 are synonym of good accuracy of the identified model. As for RERR, the smallest the value, the better accuracy. In the case of vector measurements only, the lag angle θ_{hb} of $\mathbf{h}$ with respect of $\mathbf{b}$ is computed (the smaller, the better).

2.5. Identification methods

In order to assess the effectiveness of the proposed method, identifications have been repeated with another algorithm (hereafter called "competitor") based on fitting experimental data by using a numerical minimization algorithm

[25]. More precisely, the competitor algorithm solves numerically a constrained minimization problem so as to identify a given number of cells. Conversely to the analytical method, the competitor algorithm must be fed by an adequate set of experimental measurements (loops, or other signals). In our opinion, this algorithm is representative enough of the class of identification methods based on numerical fitting.

3. Theory/Calculation

Hereafter a discrete formulation of the EB model is briefly introduced. Then, a continuous formulation of the model is derived, where discrete parameters are replaced by continuous functions. The identification method, which is based on the continuous formulation, is then presented.

3.1. Energy based model (discrete formulation)

The EB model decomposes the excitation field $\mathbf{h}$ into a reversible $\mathbf{h_r}$ and an irreversible part $\mathbf{h_i}$:

$$\mathbf{h} = \mathbf{h_i} + \mathbf{h_r} \tag{6}$$

The reversible part $\mathbf{h_r}$ is discretized as the weighted sum of $\mathbf{q}_k$ contributions of a certain number of cells N:

$$\mathbf{h_r} = \sum_{k=0}^{N-1} \omega_k \mathbf{q}_k \tag{7}$$

where the set of the weights $\{\omega_k\}$ is a partition of the unit:

$$\sum_{k=0}^{N-1} \omega_k = 1. \tag{8}$$

The term $\mathbf{q}_k$ is the internal state of the k^{th} cell. At each step, the following update rule is applied (Figure 1a):

$$\mathbf{q}_k = \begin{cases} \mathbf{q}_k^{(p)} & \text{if } ||\mathbf{h} - \mathbf{q}_k^{(p)}|| < \kappa_k \\ \mathbf{h} - \kappa^k \cdot \frac{\mathbf{h}-\mathbf{q}_k^{(p)}}{||\mathbf{h}-\mathbf{q}_k^{(p)}||} & \text{otherwise} \end{cases} \tag{9}$$

where $\mathbf{q}_k^{(p)}$ is the value of $\mathbf{q}_k$ at the previous step, and κ_k is the pinning field of the cell. It can be assumed without loss of generality that cells are ordered in such a way that $\{\kappa_k\}$ is an increasing sequence. The magnetization $\mathbf{m}$ is calculated from $\mathbf{h_r}$:

$$\mathbf{m} = M_{an}(||\mathbf{h_r}||) \cdot \frac{\mathbf{h_r}}{||\mathbf{h_r}||} \tag{10}$$

where $M_{an}(||\mathbf{h_r}||)$ is a scalar anhysteretic function. Finally the flux density $\mathbf{b}$ is obtained through:

$$\mathbf{b} = \mu_0(\mathbf{m} + \mathbf{h}). \tag{11}$$

In order to identify the model, the anhysteretic function M_{an} and the set of cells (ω_k, κ_k) must be determined.

3.2. Continuous formulation

In order to proceed, it is necessary to write the EB model into a continuous form. To this aim, observe that when the number of cells N tends to infinity, the summation (7) can be replaced by an integral:

$$\mathbf{h_r} = \lim_{N\to\infty} \sum_{k=0}^{N-1} \omega_k \mathbf{q}_k = \int_0^1 \mathbf{q}(\omega) d\omega \tag{12}$$

where $\omega_k \to d\omega$ and the sequence $\mathbf{q}_k$ is replaced by an integrable function[1] $\mathbf{q}(\omega)$. In fact, assume without loss of generality that the weights $\{\omega_k\}_{k=0}^{N-1}$ are sorted in ascending order, hence

$$0 \le \omega_1 \le \omega_1 + \omega_2 \le \ldots \le \sum_{k=0}^{N-2} \omega_k \le \sum_{k=0}^{N-1} \omega_k = 1$$

is a partition of $[0; 1]$. The function $\mathbf{q}(\omega)$ is built in such a way that $\mathbf{q}(\omega) = \mathbf{q}_k$ for any ω belonging to the k^{th} sub-interval. The measure of the k^{th} sub-interval of this partition is ω_k: hence (7) is a Riemann sum, the limit of which is by

[1] A similar approach is taken on in [26] (see equation 15 in particular) but with a different dependence of the function $\mathbf{q}$ (aka $\mathbf{h}_r^*$) which in [26] is expressed as a function of the pinning field κ.

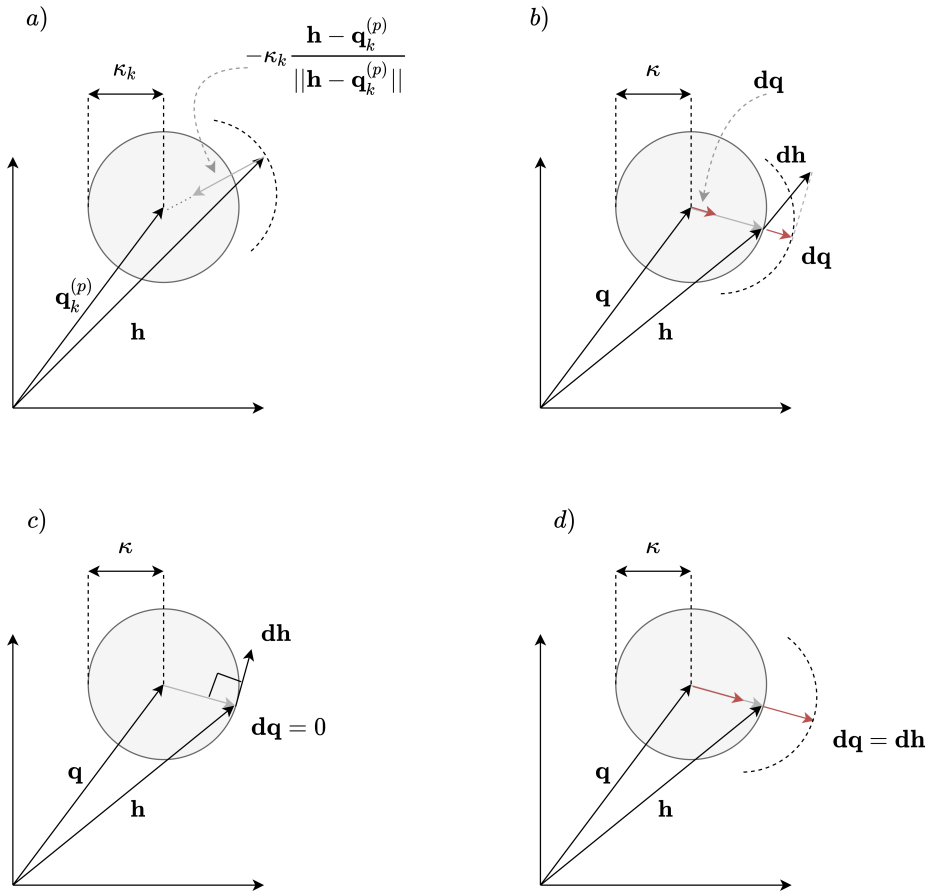

Figure 1: Cell update rule in the discrete case (a) and in the continuous case (b). In the continuous case the variation $\mathbf{dq}$ is highlighted by using red color. It is demonstrated that only the component of $\mathbf{dh}$ aligned with $\mathbf{h}-\mathbf{q}$ matters. The particular cases of $\mathbf{dh}$ perpendicular and perfectly aligned with $\mathbf{h}-\mathbf{q}$ are illustrated in (c) and (d) respectively.

definition the integral of $\mathbf{q}(\omega)$ between 0 and 1. For the sake of simplicity, hereafter the dependence on ω will be dropped.

The update rule (9) must be transformed into a differential equation. For any value of ω, until $||\mathbf{h}-\mathbf{q}|| < \kappa$, a modification of the magnetic field has no effect on $\mathbf{q}$. The case $||\mathbf{h}-\mathbf{q}|| > \kappa$ is forbidden, in that the model will modify its state so as to make this case impossible. Assume that $||\mathbf{h}-\mathbf{q}|| = \kappa$. In this case, an infinitesimal modification of the magnetic field $\mathbf{h} \to \mathbf{h}+\mathbf{dh}$ may induce a variation $\mathbf{q} \to \mathbf{q}+\mathbf{dq}$. The value of $\mathbf{dq}$ can be computed with (9) by replacing $\mathbf{q}_k^{(p)} \to \mathbf{q}$ and $\mathbf{q}_k \to \mathbf{q}+\mathbf{dq}$:

$$\mathbf{dq} = (\mathbf{h}-\mathbf{q}) + \mathbf{dh} - \kappa \frac{(\mathbf{h}-\mathbf{q})+\mathbf{dh}}{||(\mathbf{h}-\mathbf{q})+\mathbf{dh}||} \tag{13}$$

In order to find the continuous upgrade rule, it is enough to write the first-order Taylor development of (13):

$$\mathbf{dq} = \frac{(\mathbf{h}-\mathbf{q})[\mathbf{dh}\cdot(\mathbf{h}-\mathbf{q})]}{||\mathbf{h}-\mathbf{q}||^2} \tag{14}$$

In fact, the term

$$\frac{\kappa}{||(\mathbf{h}-\mathbf{q})+\mathbf{dh}||} = \frac{||\mathbf{h}-\mathbf{q}||}{||(\mathbf{h}-\mathbf{q})+\mathbf{dh}||}$$

can be linearized around $\mathbf{dh}=0$ as:

$$\frac{||\mathbf{h}-\mathbf{q}||}{||(\mathbf{h}-\mathbf{q})+\mathbf{dh}||} \simeq 1 - \frac{\mathbf{dh}\cdot(\mathbf{h}-\mathbf{q})}{||\mathbf{h}-\mathbf{q}||^2} = 1 - \frac{\mathbf{dh}\cdot(\mathbf{h}-\mathbf{q})}{\kappa^2}$$

By replacing this expression in (13) one obtains:

$$\mathbf{dq} \simeq (\mathbf{h}-\mathbf{q}) + \mathbf{dh} - \left(1 - \frac{\mathbf{dh}\cdot(\mathbf{h}-\mathbf{q})}{\kappa^2}\right)[(\mathbf{h}-\mathbf{q})+\mathbf{dh}]$$

Finally, (14) is obtained by neglecting the nonlinear terms in the latter expression. One observes that this expression is the component of $\mathbf{dh}$ aligned with the vector $\mathbf{h}-\mathbf{q}$, nothing more, nothing less (Figure 1b). That is, if $\mathbf{dh}$ is perpendicular to the vector $\mathbf{h}-\mathbf{q}$ one obtains that $\mathbf{dq}=0$ (Figure 1c). Conversely, when $\mathbf{dh}$ and $\mathbf{h}-\mathbf{q}$ are aligned (as it happens in the case of a scalar excitation) and have the same orientation, the variation $\mathbf{dq}=\mathbf{dh}$ is maximum (Figure 1d). Finally, notice that in fact the state of the model will be modified

only if $\mathbf{dh} \cdot (\mathbf{h} - \mathbf{q}) > 0$, hence the (13) must be modified as:

$$\mathbf{dq} = (\mathbf{h} - \mathbf{q}) \frac{\max([\mathbf{dh} \cdot (\mathbf{h} - \mathbf{q})], 0)}{||\mathbf{h} - \mathbf{q}||^2} \tag{15}$$

To wrap up, the update rule in the continuous case writes:

$$\mathbf{dq} = \begin{cases} (\mathbf{h} - \mathbf{q}) \frac{\max([\mathbf{dh} \cdot (\mathbf{h} - \mathbf{q})], 0)}{||\mathbf{h} - \mathbf{q}||^2} & \text{if } ||\mathbf{h} - \mathbf{q}|| = \kappa \\ 0 & \text{otherwise} \end{cases} \tag{16}$$

This expression can be rewritten equivalently as:

$$\mathbf{dq} = \begin{cases} (\mathbf{h} - \mathbf{q}) \frac{\max([\mathbf{dh} \cdot (\mathbf{h} - \mathbf{q})], 0)}{\kappa^2} & \text{if } ||\mathbf{h} - \mathbf{q}|| = \kappa \\ 0 & \text{otherwise} \end{cases} \tag{17}$$

where $\kappa = \kappa(\omega)$ is the pinning field distribution, which has to be identified. Similarly to the discrete case, it can be assumed without loss of generality that $\kappa(\omega)$ is an increasing function.

It must be observed that the case of $\kappa(\omega) = 0$ deserves a particular attention. In the discrete case, the case $\kappa_0 = 0$ represents a cell which has an anhysteretic behaviour, that is $\mathbf{q}_k = \mathbf{h}$ at any time. In the continuous case too, when $\kappa(\omega) = 0$ we have an anhysteretic behaviour, that is:

$$\mathbf{dq} = \begin{cases} (\mathbf{h} - \mathbf{q}) \frac{\max([\mathbf{dh} \cdot (\mathbf{h} - \mathbf{q})], 0)}{\kappa^2} & \text{if } ||\mathbf{h} - \mathbf{q}|| = \kappa, \quad \forall \kappa > 0 \\ \mathbf{dh} & \text{if } \kappa = 0 \\ 0 & \text{otherwise} \end{cases} \tag{18}$$

3.3. Identification

As anticipated beforehand, so as to identify the model the anhysteretic function M_{an} and the set of cells (ω_k, κ_k) must be determined. The anhysteretic magnetization $M_{an}(h_r)$ must be determined independently (for sake of completeness, a program is reported in Appendix A.2); hereafter we will focus on the parameters $\{\omega_k\}$ and $\{\kappa_k\}$ only.

The identification will be taken on in the scalar case, basing on the continuous formulation of the model. The starting point is the equation (20) of

reference [23], reported hereafter for easyness of reading:

$$h_{coer}(h_{peak}) = \frac{\sum_{k=0}^{m(h_{peak})} \omega_k \kappa_k}{\sum_{k=0}^{m(h_{peak})} \omega_k} \tag{19}$$

where $m(h_{peak})$ is the highest index k for which $\kappa_k < h_{peak}$, that is:

$$k \leq m(h_{peak}) \quad \Longleftrightarrow \quad \kappa_k < h_{peak} \tag{20}$$

Actually, it is clear from (20) that $m(h_{peak})$ contains all the information required to determine the sequence $\{\kappa_k\}$. Equation (19) holds for discrete models. In [23] the identification is taken on by fitting numerically the parameters $\{\omega_k\}$ and $\{\kappa_k\}$ of this equation basing on a discrete set of points of the curve $h_{coer}(h_{peak})$.

Our approach will be to rewrite (19) in a continuous form, and to determine an analytical expression of a distribution function $W(h_{peak})$ which is the continuous counterpart of $m(h_{peak})$, from which the distribution $\kappa(\omega)$ can be obtained. In the theoretical analysis, we assume that the continuous curve $h_{coer}(h_{peak})$ is known. From the practical point of view, the continuous curve has to be interpolated from a discrete set of points $\{(h_{coer}, h_{peak})_k\}$.

Definition of the distribution $W(h)$. The distribution $\kappa : \omega \mapsto h$ takes values of $\omega \in [0; 1]$ to the pinning field h, where it is assumed that $\kappa(\omega)$ is monotone, non decreasing. At the continuous level, $(d\omega, \kappa(\omega))$ represents an infinitesimal cell of weight $d\omega$ and pinning field $\kappa(\omega)$.

We define an auxiliary distribution $W : h \mapsto \omega$ such that:

$$\kappa(\omega) \leq h \quad \forall \omega \leq W(h) \tag{21}$$

So as to simplify the mathematical development, hereafter it will be assumed that $\kappa(\omega)$ is a monotone, strictly increasing (hence bijective) ordinary function:

$$\kappa(\omega) = h \quad \Longleftrightarrow \quad \omega = W(h) \quad \Longleftrightarrow \quad \kappa(W(h)) = h \tag{22}$$

Thus $W(h)$ becomes simply the inverse function of κ:

$$W(h) = \kappa^{-1}(h) \tag{23}$$

Notice that this is not a fundamental limitation: in the general case, where $\kappa(\omega)$ is a piece-wise continuous function, the same theoretical developments could be taken on by using the formalism of distributions. To this aim, (22) can be equivalently rewritten by using the notion of inverse image:

$$W(h) = \sup\{\kappa^{-1}([0;h])\} = \sup\{\omega : \kappa(\omega) \leq h\} \tag{24}$$

One observes that the distribution $W(h)$ is the continuous counterpart of the quantity $m(h)$ defined beforehand (20). It is also clear that the knowledge of $W(h)$ is enough to determine $\kappa(\omega)$.

The typical graphic of $W(h)$ is sketched in Figure 2. It can be foreseen that the graphic of $W(h)$ has a plateau for any $h \geq \kappa(1)$, which corresponds to the maximum pinning field of cells, that is to $\max_{\omega\in[0;1]} \kappa(\omega)$.

The value of $\frac{dh_{coer}}{dh_{peak}}\Big|_{h_{peak}=0}$ has an influence on the value of $W(0)$. In fact, if $\frac{dh_{coer}}{dh_{peak}} > 0$ for $h_{peak} = 0$, an infinitesimal modification of the magnetic field produces immediately an increment of the magnetization; hence a cell with anhysteretic behaviour exists ($\kappa_0 = 0$). In the continuous case we would have $\kappa(0) = 0$, thus $W(0) = 0$. Otherwise, if $\frac{dh_{coer}}{dh_{peak}} = 0$ for $h_{peak} = 0$ the value of $W(h)$ will be somewhere in the range $(0; 1]$.

Finally, the derivative of $W(h)$ is linked to the weights of cells, in that one has (Figure 2):

$$d\omega = \left(\frac{dW}{dh}\right) dh \tag{25}$$

That is, the weight $d\omega$ of the infinitesimal cell of pinning field $\kappa(\omega) = h$, is given by $\left(\frac{dW}{dh}\right) dh$. From the standpoint of probabilities, the function $W(h)$ is the cumulative distribution function of κ, thus its derivative is the probability of finding a cell with pinning field $\kappa \in [h, h + dh]$. The inflexion points of h, where the second derivative $\frac{d^2W}{dh^2} = 0$, correspond to the peaks (or local minima) of the weight distribution of cells.

Hypothesis. In order to proceed, we pose the following hypothesis:

a) the curve $h_{coer}(h_{peak})$ takes non negative values, it is derivable and monotone, strictly increasing for any $h_{peak} < h^{sat}_{peak}$. For any value $h_{peak} \geq h^{sat}_{peak}$

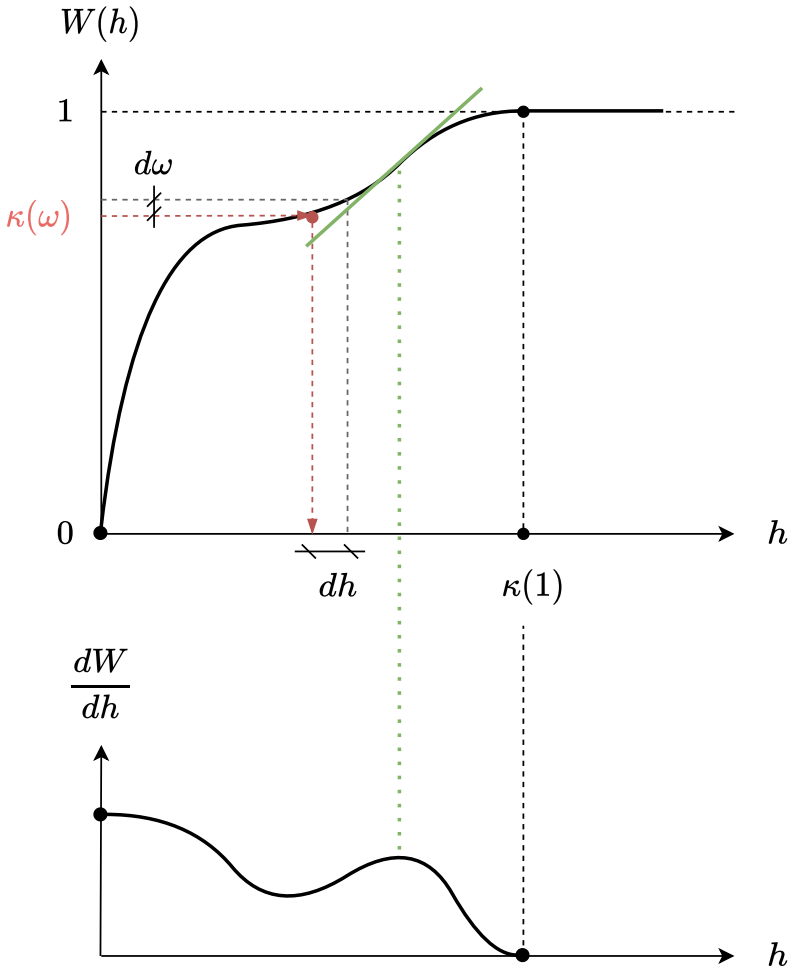

Figure 2: Sketch of the graphic of the function $W(h)$ which, in the particular case of $\kappa(\omega)$ bijective, is the inverse function of $\kappa(\omega)$. Notice the plateau for $h \geq \kappa(1)$. The derivative of $W(h)$ is linked with the weights of cells $d\omega$. In this graphic it has been supposed that $\frac{dh_{coer}}{dh_{peak}} > 0$ for $h_{peak} = 0$, and hence $W(0) = 0$, which practically means that the first cell has an anhysteretic behaviour ($\kappa_0 = 0$). The first derivative $\frac{dW}{dh}$ is representative of the weights distribution of cells, the peaks of which correspond to inflection points of the graphic of W.

the curve is saturated:

$$h_{peak} \geq h_{peak}^{sat} \qquad \Longrightarrow \qquad h_{coer} \equiv h_{coer}^{sat} \tag{26}$$

Moreover, it is assumed that the values h_{peak}^{sat} and h_{coer}^{sat} are known.

b) The distribution function $W(h)$ is derivable at any point, and $\frac{dW}{dh} > 0$ for any $h < \kappa(1)$, that is for $\omega \in [0; 1)$.

If follows from a) that the derivative $\frac{h_{coer}}{h_{peak}}$ is strictly positive, including for $h_{peak} = 0$. Thus an anhysteretic cell is necessary present, and the function $W(h)$ satisfies the following properties:

$$W(0) = 0 \qquad ; \qquad W(h_{peak}^{sat}) = 1 \tag{27}$$

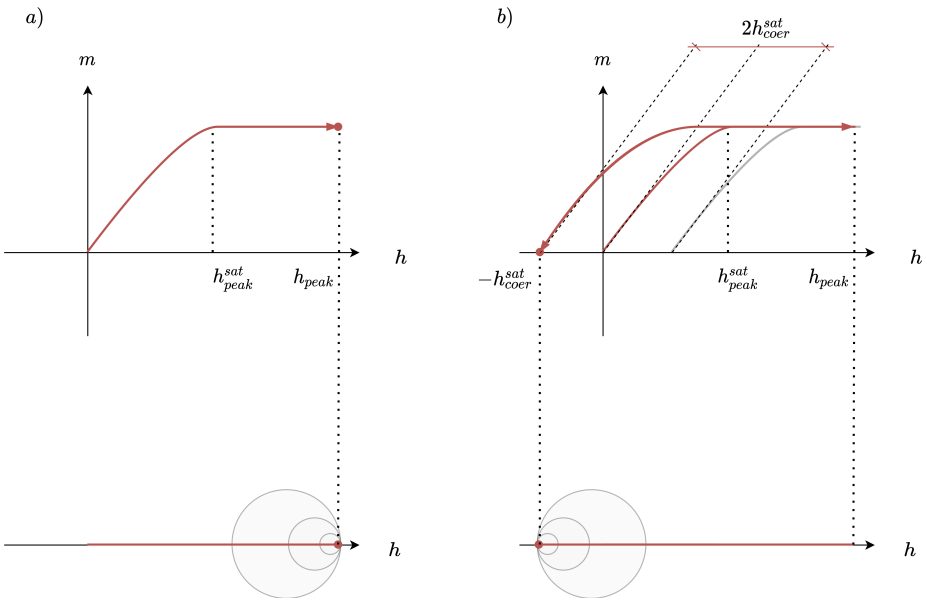

Figure 3: Sketch of a possible measurement of the curve $h_{coer}(h_{peak})$. When $h_{peak} > h_{peak}^{sat}$ all cells are activated (a). Similarly, for $h = -h_{coer}^{sat}$ all cells are activated "in the opposite direction" (b). It can be observed that, apart from the portion of the curve close to the reversal point, the width of the major cycle is constant and it is equal to $2h_{coer}^{sat}$; this is a structural property of the model.

Analytical expression of $W(h)$. To begin with, assume that the material is not fully saturated, that is $0 \leq h_{peak} < h_{peak}^{sat}$. The continuous form of (19) writes:

$$h_{coer}(h_{peak}) = \frac{\int_0^{W(h_{peak})} \kappa(\omega) d\omega}{\int_0^{W(h_{peak})} d\omega} \tag{28}$$

The integral at the denominator can be replaced by $W(h_{peak})$. According to (27) the integral at the numerator can be modified replacing $0 = W(0)$:

$$W(h_{peak}) h_{coer}(h_{peak}) = \int_{W(0)}^{W(h_{peak})} \kappa(\omega) d\omega = \int_0^{h_{peak}} h \frac{dW}{dh} dh \tag{29}$$

where we used the fact that $\kappa(W(h)) = h$. If is worth observing that this is possible because $\frac{dW}{dh} \neq 0$ (otherwise the theorem of change of variable would not hold). Also, observe that close to the saturation the distribution $W(h_{peak})$ is very flat, thus $\frac{dW}{dh} \simeq 0$. In practice, this is coherent with the physical evidence that measurement points close to the saturation take a few information for the identification of the model.

Equation (29) calls for integration by part. After a few algebraic manipulations one obtains:

$$W(h_{peak})[h_{peak} - h_{coer}(h_{peak})] = \int_0^{h_{peak}} W(h) dh \tag{30}$$

One observes that this equation is consistent with the fact that $h_{peak} > h_{coer}$ because the right hand term is a positive quantity.

Now, let's derive (30) with respect of h_{peak} so as to obtain the following differential equation, which has to be completed with an appropriate initial condition to be solved:

$$\frac{dW}{dh_{peak}} = \frac{W(h_{peak}) \frac{dh_{coer}}{dh_{peak}}}{h_{peak} - h_{coer}(h_{peak})} \tag{31}$$

We know from (27) that $W(0) = 0$, but unfortunately the Cauchy's problem composed of (31) with this initial condition admits an infinity of solutions[2].

[2] Among others, the trivial solution $W(h_{peak}) \equiv 0$. This is due to the fact that for small values of h_{peak} the denominator $h_{peak} - h_{coer}(h_{peak}) \to 0$, and hence the right hand term is not a Lipschitz continuous function. Thus the theorem of existence and uniqueness of solutions of Cauchy's problem doesn't hold (see for instance [32], chap 8.2).

Instead, let's adopt the initial condition $W(h_{peak}^{sat}) = 1$ to backwardly integrate (31) in the range $[h_{peak}; h_{peak}^{sat}]$:

$$\log W(h_{peak}^{sat}) - \log W(h_{peak}) = \int_{h_{peak}}^{h_{peak}^{sat}} \frac{\left(\frac{dh_{coer}(h)}{dh}\right)}{h - h_{coer}(h)} dh \tag{32}$$

and hence, by taking into account that $\log W(h_{peak}^{sat}) = \log 1 = 0$:

$$W(h_{peak}) = \exp\left[- \int_{h_{peak}}^{h_{peak}^{sat}} \frac{\left(\frac{dh_{coer}(h)}{dh}\right)}{h - h_{coer}(h)} dh \right] \tag{33}$$

Up to now we limited the discussion to the range $0 \leq h_{peak} < h_{peak}^{sat}$. In fact, this limitation can be removed easily by observing that for $h_{peak} \geq h_{peak}^{sat}$ the coercive field is constant, hence $\frac{dh_{coer}(h)}{dh} \equiv 0$. Thus the value h_{peak}^{sat} can be removed from (33):

$$W(h_{peak}) = \exp\left[- \int_{h_{peak}}^{+\infty} \frac{\left(\frac{dh_{coer}(h)}{dh}\right)}{h - h_{coer}(h)} dh \right] \tag{34}$$

The integrand function contains the derivative of h_{coer}, which has to be evaluated numerically. Numerical derivation, for instance by using finite differences, is always a source of numerical noise, but in practice this is not a problem because the curve $h_{coer}(h_{peak})$ has to be interpolated from a few points, and the interpolated function can be derived analytically. However, it is possible to make the derivative disappear by using $h' = h_{coer}$ as integration variable:

$$W(h_{peak}) = \exp\left[- \int_{h_{coer}(h_{peak})}^{h_{coer}^{sat}} \frac{1}{h_{peak}(h') - h'} dh' \right] \tag{35}$$

where $h_{peak}(h') \geq h'$ is the inverse function of $h_{coer}(h)$; that is, it is peak field corresponding to the coercive field $h_{coer} = h'$. This definition makes sense because until the material is not saturated the curve $h_{coer}(h_{peak})$ is bijective.

Equations (34) and (35) are perfectly equivalent, even from the numerical point of view (in the sense that they allow to compute $W(h_{peak})$ with a comparable accuracy). Once $W(h_{peak})$ is computed numerically for a large number of points, it is trivial to generate a table of $\kappa(\omega)$ by using (22), and hence to have the model identified.

3.4. Remarks

It can be observed that the expressions (34) and (35) verify (27), that is: $0 \leq W(h) \leq 1$, and in particular $W(0) = 0$ and $W(h_{peak}^{sat}) = 1$. In fact, in (34) the integrand function is positive for any $h_{peak} < h_{peak}^{sat}$, and it vanishes when the material is saturated. Hence the exponent is non positive for any value of h_{peak}, thus $W(h_{peak}) \leq 1$ and in particular:

$$W(h_{peak}^{sat}) = \exp\left[-\int_{h_{peak}^{sat}}^{h_{peak}^{sat}} \frac{\left(\frac{dh_{coer}(h)}{dh}\right)}{h - h_{coer}(h)} dh\right] = \exp(0) = 1 \tag{36}$$

On the other hand, one observes that in a neighborhood of $h_{peak} = 0$ the integral in (34) diverges [3] because $h_{coer}(0) = 0$ and hence $W(0) = 0$:

$$\lim_{h_{peak} \to 0} -\int_{h_{peak}}^{\infty} \frac{\left(\frac{dh_{coer}(h)}{dh}\right)}{h - h_{coer}(h)} dh = -\infty \quad \Longrightarrow \quad W(0) = 0 \tag{37}$$

Before analyzing the results obtained with experimental measurements, two other considerations must be anticipated. First, the result provided by the identification method are approximated, and the origin of the approximation lies in the starting equations (19) and its continuous counterpart (28). In order to understand this point, consider the behaviour of the model for low values of h_{peak}, which is sketched in figure 4. Equation (19) and (28) describe the becoming of the state of the model excited by the signal sketched in Figure 4.

[3] The demonstration is a little bit more complicated. Remember that it is assumed that $\frac{dh_{coer}}{dh_{peak}} > 0$ for $h_{peak} < \kappa(0) \leq h_{peak}^{sat}$. Hence in a neighborhood of $h_{peak} = 0$ the numerator $\frac{dh_{coer}}{dh_{peak}}$ is bounded from below by a positive, finite value a:

$$0 < a \leq \frac{dh_{coer}}{dh_{peak}}$$

For the same reason, Taylor's expansion of the function $h_{coer}(h)$ has a first-order term:

$$h_{coer}(h) = h_{coer}(0) + \left.\frac{dh_{coer}}{dh_{peak}}\right|_{h_{peak}=0} \cdot h + \circ(h) = bh + \circ(h)$$

where $b = \left(\left.\frac{dh_{coer}}{dh_{peak}}\right|_{h_{peak}=0}\right) > 0$. Hence the indefinite integral is locally of the form: $\int_0^{\infty} \frac{a}{bh} dh \to +\infty$.

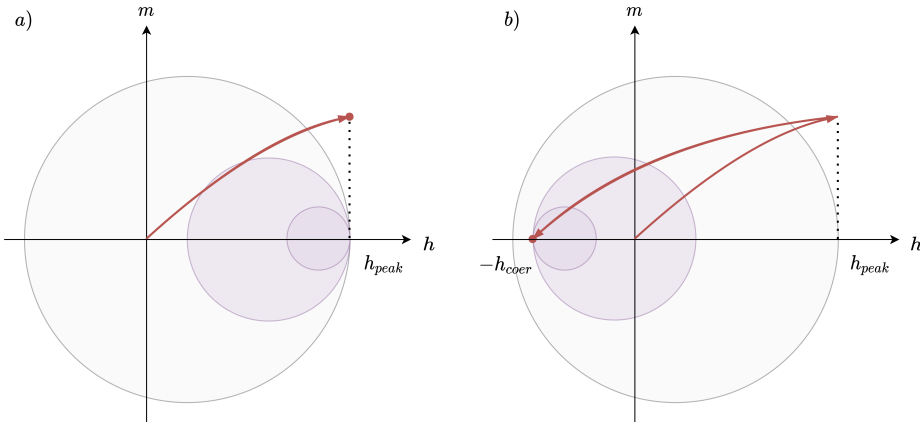

Figure 4: Sketch of a possible measurement of the curve $h_{coer}(h_{peak})$ for a low value of h_{peak} in the case of a material modeled by three cells. It can be observed that all the cells for which $\kappa \leq h_{peak}$ are activated during the ascending branch (a). Conversely, during the descending branch only cells for which $\kappa \leq h_{coer}$ are activated (highlighted in this figure), whereas the cells with $h_{coer} < \kappa < h_{peak}$ are not (b).

In the ascending branch, all the cells with $\kappa \leq h_{peak}$ are activated, and for $h = h_{peak}$ one has:

$$q = \begin{cases} h_{peak} - \kappa(\omega) & \text{if } \kappa \leq h_{peak} \\ 0 & \text{otherwise} \end{cases} \tag{38}$$

where in order to simplify the notation we given up the vector notation.

During the descending branch, when $h = -h_{coer}$ one has three different cases, so that finally the state of the material is given by:

$$q = \begin{cases} -h_{coer} + \kappa(\omega) & \text{if } \kappa \leq h_{coer} \\ h_{peak} - \kappa(\omega) & \text{if } h_{coer} \leq \kappa \leq h_{peak} \\ 0 & \text{otherwise} \end{cases} \tag{39}$$

When (39) is used in (12), by imposing that for $h = h_{coer}$ the reversible magnetic field must vanish ($h_r = 0$) one obtains:

$$0 = h_r = \int_0^{W(h_{coer})} (\kappa(\omega) - h_{coer}) d\omega + \int_{W(h_{coer})}^{W(h_{peak})} (h_{peak} - \kappa(\omega)) d\omega \tag{40}$$

It can be observed that (28) can be obtained from (40) by neglecting the second integral, that is:

$$\int_0^{W(h_{coer})} (\kappa(\omega) - h_{coer}) d\omega = 0 \tag{41}$$

Hence, (34) and (35) are approximated solution of (40). Unfortunately so far no analytical solution could be found for (40). It can be observed that the discrepancy between (41) and (40) is significant only for weak values of h_{peak} (compare figure 3 and 4), hence we expect to obtain mixed results when materials are excited with low magnetic fields. However, it has been reported that for low magnetic fields the EB model provides mixed results also with other identification methods [28].

Second, consider again the behaviour of the material when it is fully saturated. When $h_{peak} \geq h_{peak}^{sat}$, it can be deduced from (41) and(27) that the coercive field $h_{coer} = h_{coer}^{sat}$ writes:

$$h_{coer}^{sat} = \int_0^1 \kappa(\omega) d\omega \tag{42}$$

The same consideration holds for the symmetric part of the major loop, hence the width of the major loop Δh is:

$$\Delta h = 2h_{coer}^{sat} = 2 \int_0^1 \kappa(\omega) d\omega \tag{43}$$

The point is that in the major loop all of the cells are active, and hence the width of the major loop is bound to be constant at any point (figure 3b), apart from a neighborhood of reversal points where cells are not all active. The constantness of the width of the major loop is a structural property of the EB model; that is, it does not depend on the identification method.

3.5. Implementation

The numerical evaluation of (34) and (35) has been implemented in a MATLAB/Octave function (see Appendix A.1). The program accepts as input two vectors `Hc` and `Hp` which store respectively the measured values of h_{peak} and

h_{coer}, and returns two vectors `omega` and `kappa` which store respectively the estimated values of $\{\omega_k\}$ and $\{\kappa_k\}$. When using real measurements, precautions must be taken in order to avoid some pitfalls:

1) in theory the curve $h_{coer}(h_{peak})$ is monotone, but in practice this is not necessarily the case, due to measurement errors and/or electrical noise. Unfortunately this property must absolutely be verified, so that it is necessary to enforce it by sorting the vectors `Hc` and `Hp`. This is of course a "quick and dirty patch", but up to our experience it is enough to solve this issue.

   Eventually, the vector `Hc` can be perturbed by adding a negligible quantity (order of magnitude: 100ϵ, with $\epsilon \simeq 10^{-16}$ = machine precision in double precision floating point arithmetic), so as to strictly enforce the monotonicity.

2) The couple of values $h_{peak} = 0$ and $h_{coer} = 0$ are added to the data set, and eventual duplicate measurement points are removed.

3) In practice, the value of h_{coer}^{sat} is estimated as the maximum of `Hc`.

4) The curve $h_{coer}(h_{peak})$ must be interpolated. It has been observed that close to the saturation the curve becomes very flat. This kind of situation may be problematic for the interpolation algorithms. In particular, with some kinds of interpolation methods nonphysical spurious maxima are observed close to the saturation, where the curve becomes very flat.

   In order to avoid these artifacts, it may be advisable to use the simple piecewise linear interpolation, which has the defect of ensuring the continuity C^0 only (that is: the interpolated curve is continuous, but not its first derivative). Another solution is to use more complex interpolation methods (piecewise cubic, spline interpolation) which ensures at least C^1 continuity, with the precaution of removing the measurement points where the material is fully saturated and the curve $h_{coer}(h_{peak})$ becomes very flat. Remember that there points close to the saturation take little or no additional information to the model, thus in practice they can be safely removed.

We stress that, up to our experience, this pre-processing phase is crucial to obtain good results.

When (34) is used to compute $W(h)$, the derivative $\frac{dh_{coer}(h)}{dh}$ can be computed numerically by using Finite Differences. The distribution function $W(h_{peak})$ is sampled on a large number of points N (order of magnitude: $N = 1000$) which span the range $[0, \max(h_{peak})]$. Integrals in (34) or (35) are computed numerically by using standard adaptive quadrature formulas available in practically all softwares. The first sample $W(0) = 0$ is enforced in the code, because in this case the integral in (34) and (35) diverges. The final step is to compute `omega` and `kappa` basing on the computed samples of $W(h_{peaks})$. The weights of all cells are fixed to the constant value $\omega_k = \frac{1}{N}$.

Finally, it has to be pointed out that the proposed identification method returns a model composed of a number of cells which is prohibitive for practical applications. However, simplified models can be easily be generated. A simple and effective clustering algorithm is proposed in Appendix A.3.

4. Results

4.1. Ferrite 3C90

The model has been identified with the proposed method by using the values of h_{coer} and h_{peak} measured with 13 centered minor loops (Table 1). The

Table 1: Measurement points for the ferrite 3C90 (unit: A/m)

h_{peak}	9.96	19.9	29.8	40.5	50.0	59.9	69.9	79.8	90.3	100	150	199	231
h_{coer}	0.912	2.72	4.26	6.81	8.19	9.75	10.8	11.0	11.7	11.8	11.8	12.4	12.6

measurement points, together with the curve $h_{coer}(h_{peak})$ interpolated by using the piece-wise linear interpolation and the coercive field h_{coer} approximated by using (19) are plotted in Figure 5a. The distribution function $W(h)$ is plotted

in Figure 5b. It can be observed that starting from $h = 100$ A/m the material is saturated, hence $W(h)$ is close to 1.

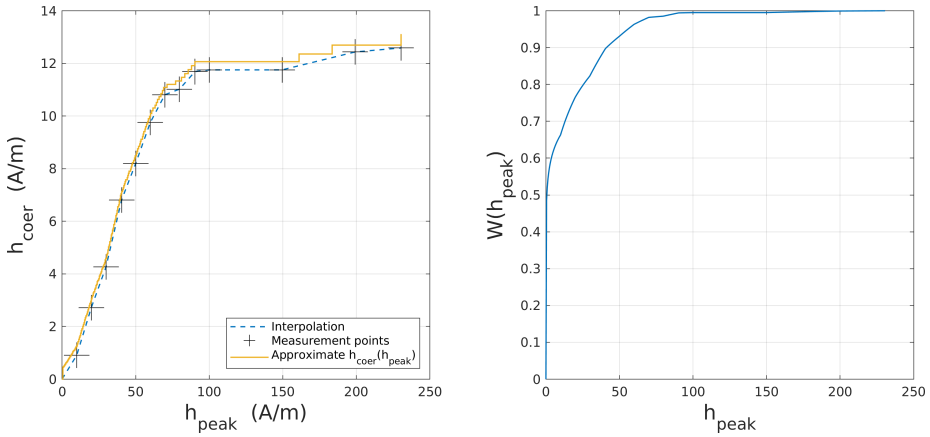

Figure 5: a) Measurement points $h_{coer}(h_{peak})$ (+) and piece-wise linearly interpolated curve (dashed line). The staircase curve represent the approximate computation of h_{coer} by using (19) with the identified model. b) Distribution function $W(hpeak)$, from which the pinning field $\kappa(\omega)$ is computed.

The model has been first identified with $N = 512$ cells, which have then been clustered into 10 cells by using the algorithm described in Appendix A.3. The measured loops have been simulated by using both models (with 512 and 10 cells and are plotted Figure 6. The table 2, gives the different indicators for each loop minor centered loop. The same loops have been used to identify the material with the competitor algorithm.

In Figure 7 is depicted a signal composed of the fundamental harmonic and the third harmonic, which gives rise to minor loops. This measurement is not part of the dataset used to identify the model.

4.2. TEAM32 laminations

For the TEAM32 laminations, the model has been identified by using the values of h_{coer} and h_{peak} obtained from centered minor loops measured along the rolling direction (Table 3). One observes that the last point ($h_{peak} = 5442$ A/m, $h_{coer} = 84.9$ A/m) is clearly an outlier. Nevertheless the identification method

Table 2: Indicators for the 3C90 ferrite

$\max \lvert h \rvert$ (A/m)	RBMAX	RPOW	RERR	RHCOE	RBREM
10	1.21	1.81	28%	1.10	1.41
30	1.11	0.73	10%	0.76	0.80
50	1.04	0.64	7%	0.74	0.67
90	0.99	0.75	4%	0.89	0.82
150	0.99	0.87	2%	0.96	0.94
230	0.99	0.94	1%	1.02	0.99

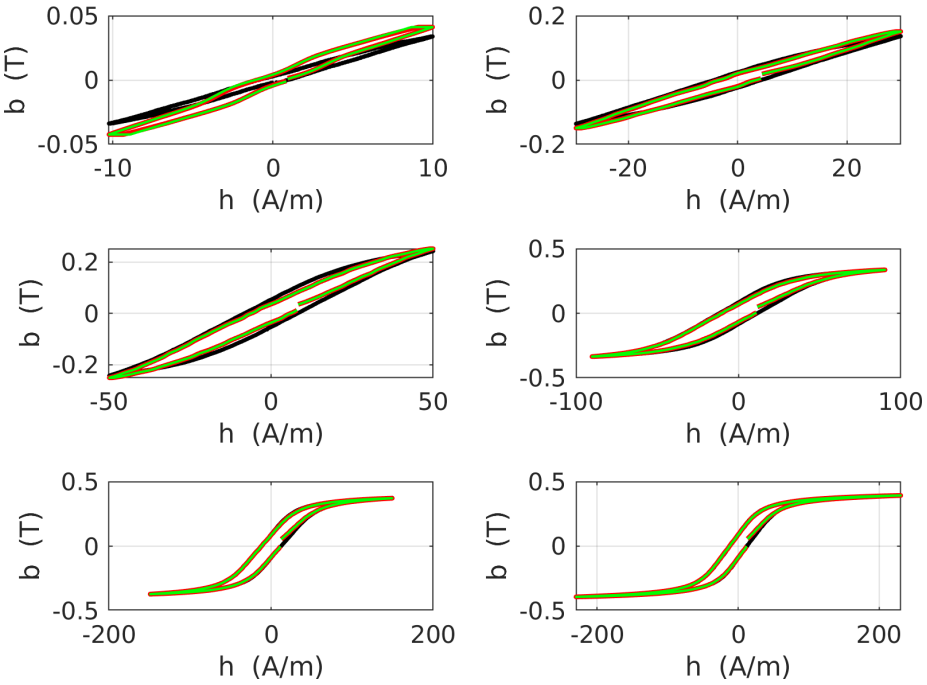

Figure 6: Ferrite 3C90: measured loops of increasing amplitude (black points). The same loops have been simulated with the estimated model with 512 cells (red) and 10 cells (green).

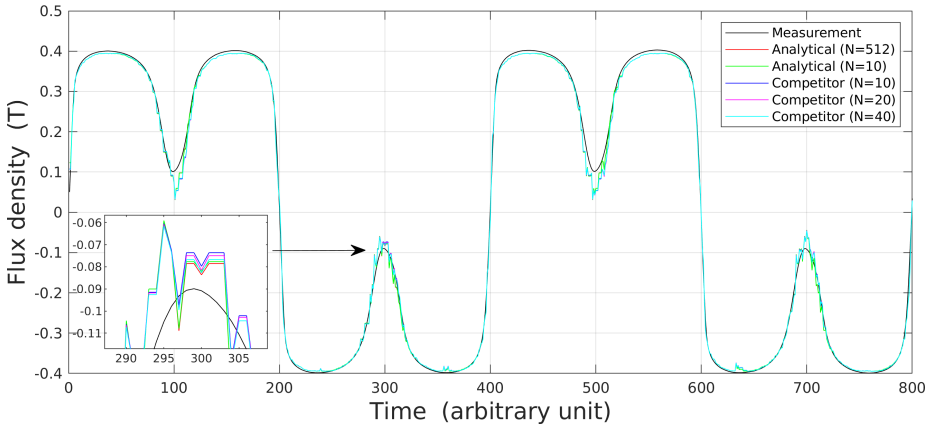

Figure 7: Signal with third harmonic measured (black) and simulated with the models identified by using the analytical algorithm (red, green) and the competitor algorithm (blue, cyan, magenta). The simulated signals are nearly superposed; they can hardly be distinguished in the inset which represents a zoom around $t = 300$.

provided a workable model. The same loops have been used to identify the material by using the competitor algorithm.

Table 3: Measurement points for the TEAM32 laminations (angle = 0°, unit: A/m)

h_{peak}	42.9	51.5	74.0	109.0	202.7	251.8	348.4	492.6	727.5	906.3	1233	5442
h_{coer}	21.3	30.6	42.7	50.3	55.1	56.9	59.8	61.1	61.3	61.6	61.9	84.9

We present some of the measured and simulated loops for increasing amplitudes in the rolling direction. The quantitative indexes for the proposed method are reported in the table 4 for these loops. In order to assess its predictive capability, the identified model has been used to simulate the loops measured in the transverse direction (Figure 9). The corresponding quantitative indicators for the proposed method for fields transverse to the rolling direction for different amplitudes are reported in Table 5.

Next, the loops measured at 90° with respect of the rolling direction have been used for the identification, and the other loops have been used to assess

Table 4: Indicators for the TEAM32 steel (angle = 0°)

$\max \lvert h \rvert$ (A/m)	RBMAX	RPOW	RERR	RHCOE	RBREM
51	0.78	0.75	25%	0.78	0.79
109	0.95	0.99	24%	1.00	0.93
252	0.98	0.96	16%	1.05	0.88
493	0.99	0.87	15%	1.06	0.84
906	0.98	0.81	12%	1.08	0.81
5442	1.00	0.60	11%	0.95	1.24

Table 5: Indicators for the TEAM32 steel (angle = 90°)

$\max \lvert h \rvert$ (A/m)	RBMAX	RPOW	RERR	RHCOE	RBREM
62	1.84	2.48	97%	1.13	2.44
76	1.71	2.06	81%	1.03	2.04
182	1.17	1.11	33%	0.90	1.23
476	1.06	0.86	26%	0.85	1.01
1284	1.04	0.74	21%	0.86	0.97
5549	1.02	0.80	10%	1.09	2.25

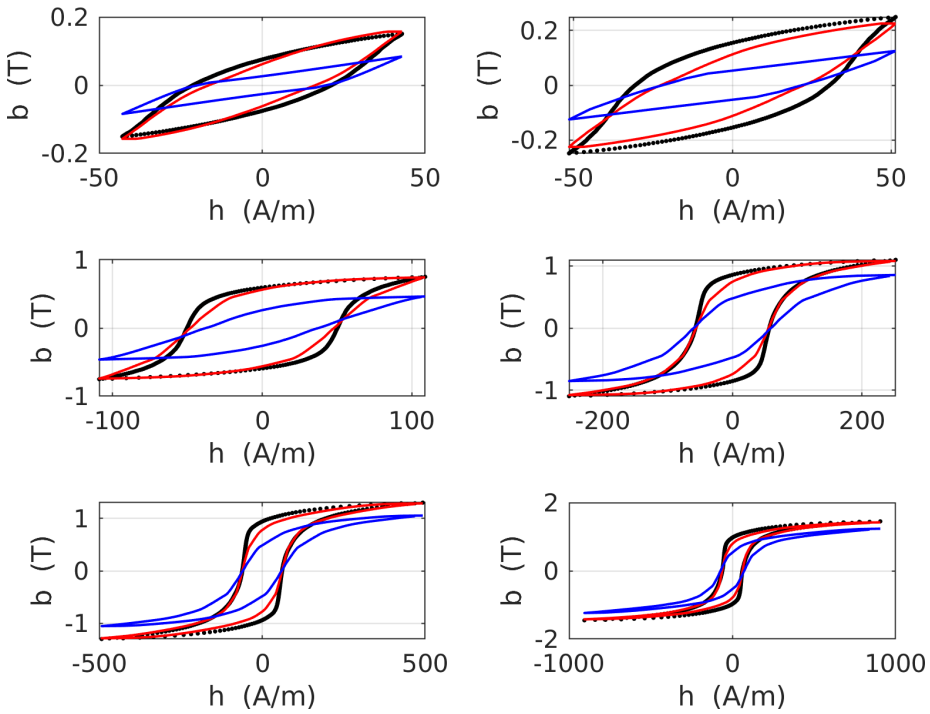

Figure 8: TEAM 32 laminations, angle = 0°: measured loops of increasing amplitude (black points) and simulated with the model identified with the proposed method (red) and with the competitor (blue). The model has been identified by using the measured loops at 0° with respect of the rolling direction.

the predictive capability. In fact it is observed that the measured loops for high values of h_{peak} intersect, thus the curve $h_{coer}(h_{peak})$ is not monotone (Table 6). Nevertheless the identification algorithm provides a workable model of the material. The indicators computed with all the available measurements are close to those already presented (data not shown).

4.3. Non-oriented grain electrical steel

In all the measurements the flux density is imposed. The model has been identified with the proposed algorithm and with the competitor algorithm by using the uni-axial loops measured along the rolling direction. The loops and the curve $h_{coer}(h_{peak})$ are not shown here but the corresponding quantitative

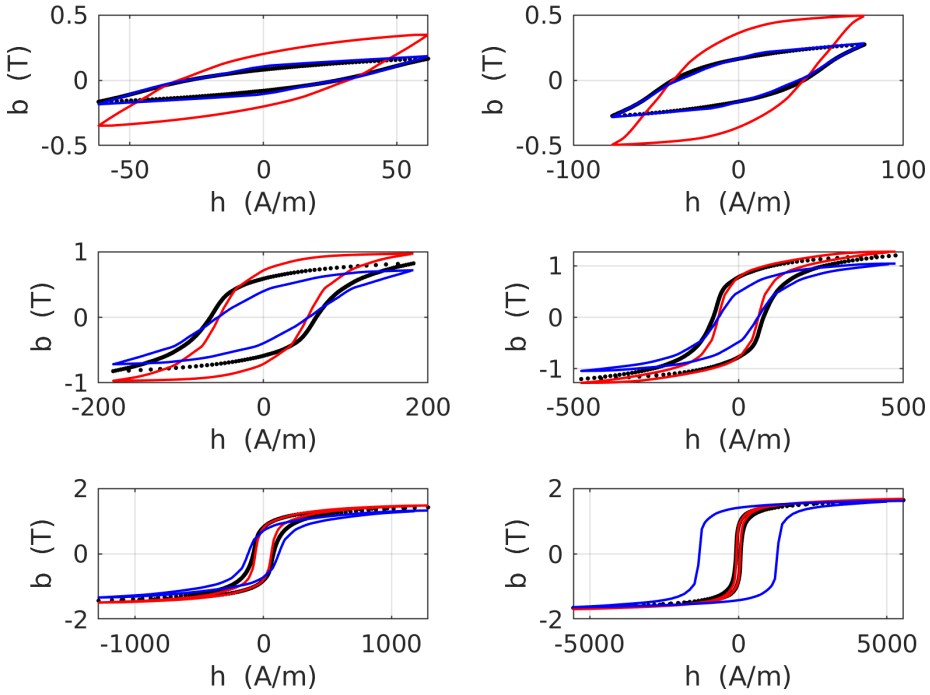

Figure 9: TEAM 32 laminations, angle = 90°: measured loops of increasing amplitude (black points) and simulated with the model identified with the proposed method (red) and with the competitor (blue). The model has been identified by using the loops measured along the rolling direction.

Table 6: Measurement points for the TEAM32 laminations (angle = 90°, unit: A/m)

h_{peak}	61.7	76.4	118.5	182.2	359.5	476.1	722.4	1284.4	2609.7	5549
h_{coer}	28.1	39.6	54.6	64.1	73.8	76.0	80.8	77.8	79.8	75.0

indicators are reported in Table 7

Table 7: Indicators for the non-oriented grains electrical steel [30] (angle = 0°)

max $\|h\|$ (A/m)	RBMAX	RPOW	RERR	RHCOE	RBREM
33	1.00	1.14	13%	1.05	1.29
47	0.88	0.78	14%	0.87	0.82
68	0.92	0.86	10%	1.00	0.92
101	0.99	0.96	6%	1.03	0.96
162	1.01	0.99	5%	1.05	0.97
295	1.01	1.00	4%	1.07	1.00
872	1.00	0.86	3%	1.09	1.12
3782	1.00	0.73	2%	1.07	1.37

Also the identified model has been used to predict the outcome of other measurements. First, in Figure 10 is depicted the flux density (left) and the magnetic field (right) in the case of an uni-axial excitement with an angle of 30° with respect of the rolling direction. The corresponding quantitative indicators are reported in Table 8.

Also the case of a circular flux density is considered. A circular flux density has been imposed experimentally. The measured and simulated loops, together with the corresponding lag-angle θ_{hb} are plotted Figure 11. The corresponding quantitative units are reported in Table 9.

Table 8: Quantitative for the non-oriented grains electrical steel [30] (angle = 30°)

max $\|\|\mathbf{h}\|\|$ (A/m)	RBMAX	RPOW	RERR
31	0.92	1.02	13%
45	0.82	0.72	21%
62	0.83	0.78	19%
95	0.93	0.95	12%
150	0.97	1.01	9%
264	0.98	1.01	6%
506	0.97	0.92	6%
1812	0.96	0.71	6%

Table 9: Quantitative for the non-oriented grains electrical steel [30] (circular flux density)

max $\|\|\mathbf{h}\|\|$ (A/m)	RBMAX	RPOW	RERR
36	1.40	1.03	31%
50	1.12	0.74	24%
73	1.15	0.88	21%
121	1.18	1.02	18%
201	1.13	1.04	13%
270	1.09	1.01	11%
373	1.06	0.95	8%
581	1.03	0.86	7%
1212	1.01	0.74	5%
1834	1.01	0.73	4%
295	1.01	0.77	3%

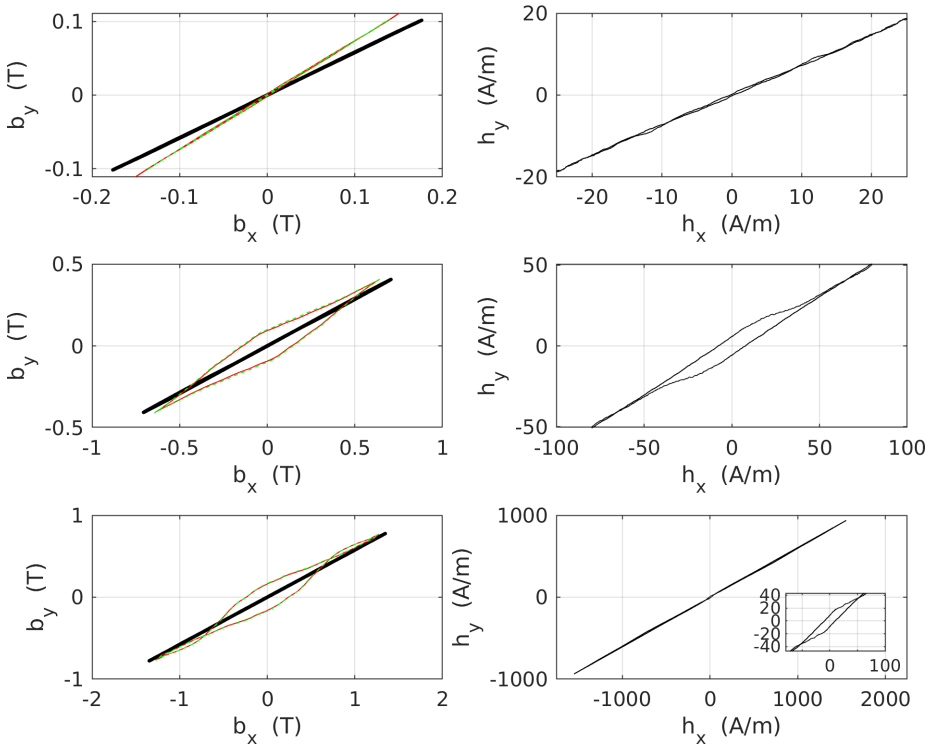

Figure 10: Flux density (left) and magnetic field (right) for an uniaxial excitation with n angle of 30° with respect of the rolling direction: measurement (black), simulation with the model identified by using the proposed method (red) and by using the competitor algorithm (green). No significant difference can be observed between the two identification models. The inset in the bottom left graphic magnifies a tiny loop close to the origin ($||\mathbf{h}|| \simeq 0$).

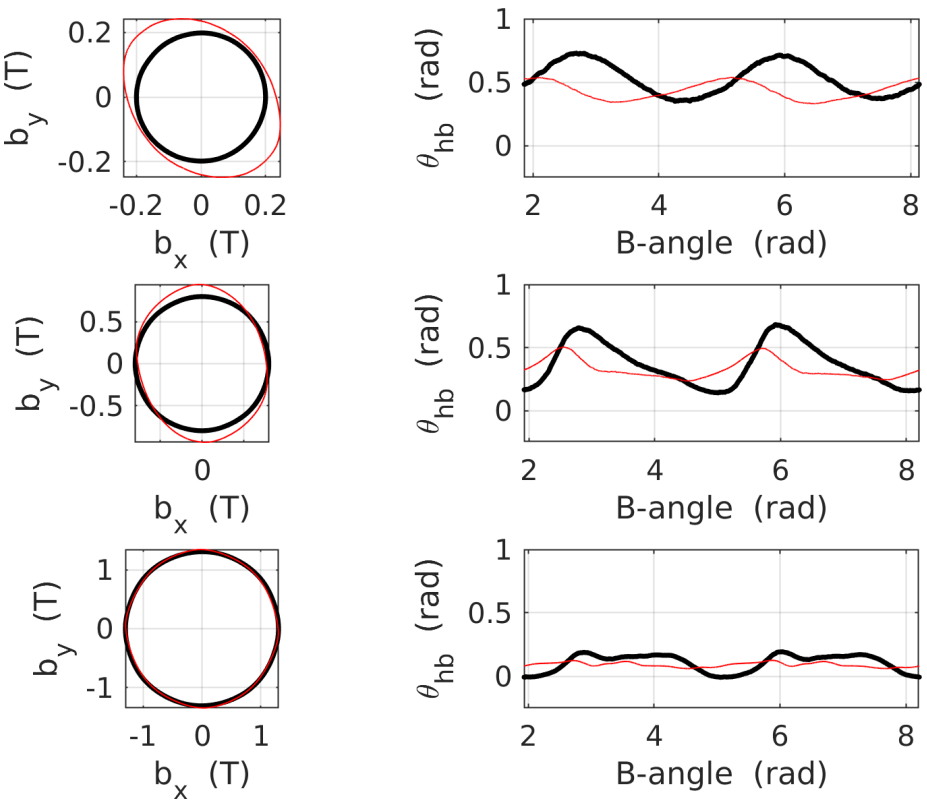

Figure 11: Flux density loops (left) and lag-angle θ_{hb} (right) for a vector excitation: measurement (black), simulation (red).

5. Discussion

5.1. Ferrite 3C90

From Figure 5a and 5b, it can can be observed that (19) provides a fairly good approximation of the coercive field.

From Figure 6, it can be observed that the original model and the model composed of only 10 cells provide practically the same result. As previously anticipated, high amplitude loops are better represented by the model than low amplitude one (Table 2). However, the difficulty of modeling low amplitude signals with this same material has already been pointed out in [28], and cannot be imputed to the identification method.

It can be observed from Figure 7 that the identified model can reproduce with good accuracy the signal, even if a higher discrepancy is observed close to the tip of the minor loop. For this signal some of the quantitative indicators are: RBMAX = 0.98, RPOW = 0.98, RERR = 4% (in this case RHCOE and RBREM cannot be evaluated).

5.2. TEAM32 laminations

The same trend observed with the 3C90 ferrite is found. When the model is identified with the proposed method by using the measurements at 0° with respect of the rolling direction, low amplitude loops are reproduced less accurately with respect to high amplitude ones (see Table 4). It is observed that the model is able to predict the measurements at 90° with an acceptable accuracy, apart from the low amplitude cycles (Table 5).

However, a more careful analysis puts in evidence a difference with respect of the 3C90 ferrite: when the amplitude of loops is increased the rms error (RERR) and the ratio between simulated and measured loops areas (RPOW) don't converge to their optimal values. This fact can be explained at least partially by observing that the width of the major loop Δh is not constant (Figure 3b). In fact, for $b = 0$ we have $\Delta h = 2h_{coer}^{(sat)} = 162$ A/m, whereas for $b = 1.2$ T the measured width $\Delta h = 307$ A/m is nearly the double (Figure

12, right). As discussed in 3.4, the constantness of the width of the major loop far from the reversal points is a structural property of the energy-based model, which is not fulfilled by this material. Hence it is natural that some discrepancies between measurements and simulations appear. This fact is also responsible for the values of RBREM, which are not as good as in the case of the 3C90 ferrite (compare Tables 2 and 4).

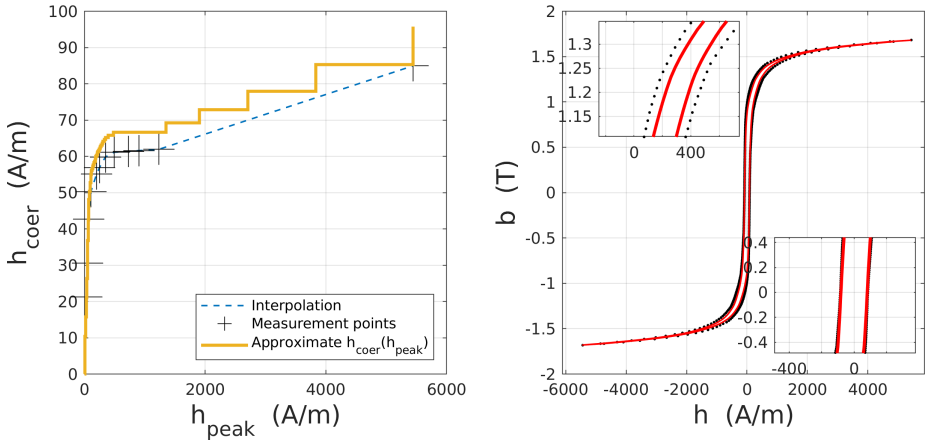

Figure 12: TEAM 32 laminations. Left: points $h_{coer}(h_{peak})$ measured at 0° with respect of the rolling direction (+) and piece-wise linearly interpolated curve (dashed line). It can be observed that a plateau of h_{coer} is achieved at about $h_{peak} = 500$A/m, suggesting that the material is already saturated. The last measurement point $h_{peak} = 5442$A/m is most likely an outlier. Right: measured loops of amplitude $h_{peak} = 5442$A/m (black points) and simulated with the estimated model (512 cells, red). The two insets magnifies the graphics around $b = 0$ and $b = 1.2$ T.

Another fact which deserves to be pointed out is that the point of the curve $h_{coer}(h_{peak})$ corresponding to the major loop ($h_{peak} = 5442$A/m) is likely to be an outlier with respect of the other points (Figure 12, left). In spite of the presence of this outlier, the identified model has a good predictive capability.

The results obtained when the model is identified by using the measurements at 90° are similar (data not shown). In this case, one observes that the experimental curve $h_{coer}(h_{peak})$ is not monotonous, which can be easily explained by measurement noise. Nevertheless, the identified model is workable and has a

good predictive capability.

5.3. Non-oriented grain electrical steel

As for the case of TEAM32 steel, the width of the major loop $\Delta h \in [78\,;202]$ A/m is not constant, and this explains the discrepancy on the losses (RPOW) between simulations and measurements in the Table 7.

Also from Figure 10, it can be seen that the material is not perfectly isotropic, as it can be noticed by the small loops for weak magnetic fields. These loops become evident in the simulated flux density (right), because the EB model is perfectly isotropic.

No practical difference is observed by repeating the simulations with the model identified with the competitor algorithm. This suggests that the origin of the observed discrepancy is the isotropic nature of the model itself. Similar considerations can be done by exploiting the other available uni-axial measurements.

Finally for the case of a circular flux density (Figure 11 and Table 9). First, it can be seen from Figure 11, that the lag angle decreases when the amplitude of loops increases, as it was pointed out in [30]. It can be observed also that the model, in this present form is unable to reproduce the becoming of θ_{hb}. Nevertheless, apart from the lag-angle, the same behaviour of the previous materials is observed (Table 9).

5.4. Comparison with another identification algorithm

In order to assess the effectiveness of the proposed method, we repeated the identification with another algorithm (competitor) based on fitting experimental data by using a numerical minimization algorithm [25]. More precisely, the competitor algorithm solves numerically a constrained minimization problem so as to identify a given number of cells. Conversely to the analytical method, the competitor algorithm must be fed by an adequate set of experimental measurements (loops, or other signals). In our opinion, this algorithm is representative

enough of the class of identification methods based on numerical minimization of a cost function.

The ferrite 3C90 has been has been identified by using both the analytical method ($N = 512$ cells, then clustered to 10 cells only) and the competitor algorithm ($N = 10$, $N = 20$, $N = 40$ and $N = 80$ cells) by using the centered minor loops. The signal with the third harmonic has been used to compare the accuracy of the two algorithms.

The computational time to identify the materials with the analytical method is of about $T_a = 0.60$ sec. On the same computer (PC Linux Fedora 34, Intel Core i7-8850H, 128 Gb of RAM) and with the same programming language (Matlab version 2020b), the competitor algorithm takes $T_{c,10} = 114$ sec with only $N = 10$ cells, $T_{c,20} = 9$ min with $N = 20$ cells and $T_{c,40} = 19.6$ min with $N = 40$ cells. For $N = 80$ cells the competitor algorithm failed to converge to the required accuracy after 42 min ; this problem could eventually be solved at the price of a much higher computational time by using appropriate strategies (multiple starting point search, increasing the maximum number of iterations, etc.).

The simulations taken on with the signal with third harmonic are depicted in Figure 7 together with the measurement. It can be easily observed that the accuracy is practically identical for the models identified with the analytical and with the competitor algorithm.

In the case of TEAM32 laminations, the material has been identified by using the competitor algorithm ($N = 20$ cells). The algorithm executed in $T_{c,20} = 20$ min and failed to converge up to the required accuracy, whereas the proposed algorithm required less than 1 sec. The slowness and the non convergence of the competitor algorithm can be explained by the fact that, as already mentioned, for the TEAM32 steel the width of the major loop is not constant, which is a structural property of the model, and hence cannot be reproduced by the EB model.

The identified model with the competitor has a predictive capability quite

different from the one identified by using the proposed algorithm (Figure 9). It can be observed that the competitor predicts better the loops of low; conversely the loop corresponding to high fields is completely wrong. This may be related to the presence of the outlier in the curve $h_{coer}(h_{peak})$, which in turns has only a moderate effect on the proposed algorithm.

In the case of non-oriented grains electrical steel, a model composed of 20 cells has been successfully identified, starting from the same dataset. The simulations executed with this second model is also plotted in Figure 10: like in the case of the ferrite 3C90, no significant difference is observed in the predictive capability for the two models. Conversely, the competitor algorithm requires a much larger computational time with respect of the proposed method.

6. Conclusion

The purpose of this work is to present a new identification method for the EB model of magnetic hysteresis. Conversely to other identification methods, the proposed method is based on analytical formulas which allows to compute a distribution function $W(h)$ from the curve $h_{coer}(h_{peak})$, from which the pinning field of cells κ_k is easily computed. A simple clustering algorithm allows to simplify the model by reducing the number of cells. The computational routines in MATLAB/Octave are very short, and are listed in the appendix.

The proposed method has several advantages. The identification is taken on with no free fitting parameters: that is, no minimization step is required. This completely removes convergence issues which are often observed with minimization algorithms. Moreover, the proposed algorithm requires no critical tuning, conversely to minimization algorithms where some parameters need to be carefully set (i.e. max. number of iterations, starting point, target tolerance etc.).

From the standpoint of the computational time, the proposed algorithm outperforms by several order of magnitude other algorithms based on numerical minimization, while providing a comparable accuracy. On the other hand, it has

to be said that the proposed method requires as input the curve $h_{coer}(h_{peak})$, whereas other algorithms can be fed with many other kinds of signals, and hence are more flexible.

From the standpoint of the prediction capability, no major differences are observed between the proposed algorithm and other algorithms, provided that the minimization algorithm converges.

Most importantly, it is demonstrated that the identification method is quite robust, even in the presence of measurement noise or outliers in the measured points $\{(h_{coer}, h_{peak})_k\}$.

The identification method has been tested with three different materials, and in all cases it has demonstrated a good predictive power. Some limitations on the accuracy of the results have been put in evidence. In particular, simulations provided mixed results for low amplitude fields, and were unable to reproduce the becoming of the lag angle between **h** and **b** in vector measurements. However, similar limitations are imputable to the EB model itself rather than to this or indeed any other identification methods.

The problem of the accurate prediction of the lag angle remains an open problem with any model of vector hysteresis, not only the EB model. In particular, as much as the EB model is concerned, the modeling of anisotropic materials is still in its infancy and deserves further investigations. For sure, one aspect of this problem is the identification of models by using vector measurements. It can been foreseen that using vector measurements for the identification will improve the predictive capability. In our opinion, the prediction of the lag angle should be studied first (model extension/modification) before questioning the identification method.

Appendix A. Programs

The MATLAB/Octave functions reported hereafter implements the identification algorithm, the estimation of the anhysteretic curve, and a simple clustering algorithm to reduce the number of cells of the model. The functions has been tested with both MATLAB (version 2020b) and Octave (version 5.2).

Appendix A.1. Identification

The function `identify` listed hereafter implements the identification algorithm. The function requires as input arguments the measured values of the coercive field (`Hc`) and peak field (`Hp`) and the number of cells (`N`), and returns the weights (`omega`) and the pinning fields (`kappa`) of cells. The hard-coded variable `FRM` allows to select which formula between (34) (`FRM=1`) and (35) (`FRM=2`) is used to compute the distribution function $W(h)$.

```
function [omega, kappa] = identify (Hc, Hp, N)
FRM = 1 ; Hp = [0 ; Hp(:)] ; Hc = [0 ; Hc(:)];
Hp = unique(Hp) ; Hc = sort(Hc); max_Hp = max(Hp) ; max_Hc = max(Hc);
Hc = Hc + 100*eps*(0:numel(Hc)-1)';
fun_Hc = @(h) interp1(Hp, Hc, h, 'linear', max(Hc));
fun_dHc = derive(fun_Hc);
fun_Hp = @(h) interp1(Hc, Hp, h, 'linear', 'extrap');
Hp_ = linspace(0, max_Hp, N);
W = zeros(N, 1);
for k = 2 : N
  if FRM == 1
    W(k) = exp(-integral(@(h) fun_dHc(h) ./ (h - fun_Hc(h)), Hp_(k), max_Hp));
  else
    W(k) = exp(-integral(@(h) 1./(fun_Hp(h) - h), fun_Hc(Hp_(k)), fun_Hc(max_Hp)));
  end
end
kappa = w2kappa(Hp_, W);
omega = ones(N, 1) / N;
end

function dF = derive(F)
dx = 1E-4 ; dF = @(x) (F(x+dx) - F(x)) / dx;
```

```
end

function kappa = w2kappa(Hp, W)
N = numel(W) ; Omega = linspace(0, 1, N) ; Omega = Omega(:);
kappa = zeros(N, 1) ; t = 1;
for k = 1 : N
   while(t <= N  &&  Omega(t) <= W(k))
      kappa(t) = Hp(k) ; t = t + 1;
   end
end
end
```

Appendix A.2. Estimation of the anhysteretic curve

The function `anhysteretic` estimates the anhysteretic curve from a set of scalar measurements of the magnetic field ($\{h_k\}$, input argument `H`) and flux density ($\{b_k\}$, input argument `B`), from which the magnetization $\{m_k\}$ is computed. The measurement points can be provided in any order, and can represent any kind of signal, provided that the major loop is explored. The program reconstructs the major loop by generating the envelope of the points. More precisely, the set of points on the ascending branch of the major loop are selected basing on the following criterion (Figure A.13):

$$\text{find } k \text{ such that: } m_k \geq m_j \text{ and } h_k \leq h_j \quad \forall j \neq k \tag{A.1}$$

A similar criterion is used to identify the descending branch:

$$\text{find } k \text{ such that: } m_k \leq m_j \text{ and } h_k \geq h_j \quad \forall j \neq k \tag{A.2}$$

All the other measurement points are discarded. After that the points on the ascending and descending branches have been identified, the two branches are interpolated by using a fixed number of point (hard-coded variable `nb = 64`), and the anhysteretic curve is estimated as the median line between the ascending and the descending curve. The function returns the samples of the anhysteretic curve (`Ha`, `Ma`) and the handle to a function (`fn`) which evaluates the anhysteretic magnetization as a function the magnetic field.

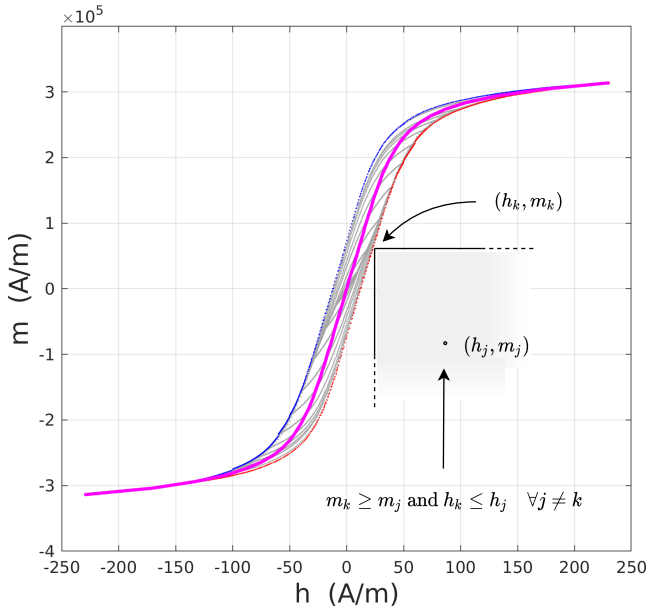

Figure A.13: Sketch of the algorithm to estimate the anhysteretic curve. The ascending and descending branches are depicted in red and blue color respectively. The estimated anhysteretic curve is plotted in magenta.

```
function [Ha, Ma, fn] = anhysteretic(H, B)
nb = 64 ; H = H(:) ; B = B(:) ; mu0 = pi*4.0e-7 ; M = B/mu0 - H;
minH = min(H) ; maxH = max(H) ; ind_a = [] ; ind_d = [];
for n = 1 : numel(H)
  if isempty(find(H > H(n)  &  M < M(n)))
    ind_a(end+1) = n;
  elseif isempty(find(H < H(n)  &  M > M(n)))
    ind_d(end+1) = n;
  end
end
[ha, ma] = preprocessing(H(ind_a), M(ind_a));
[hd, md] = preprocessing(H(ind_d), M(ind_d));
Ma = linspace(max(min(ma), min(md)), min(max(ma), max(md)), nb);
Hai = interp1(ma, ha, Ma) ; Hdi = interp1(md, hd, Ma);
Ha = (Hai + Hdi) / 2.0 ;
Ha = [ min(H) Ha max(H) ] ; Ma = [ min(M) Ma max(M) ];
[Ha, Ma] = preprocessing(Ha, Ma);
```

```
fn = @(h) interp1(Ha, Ma, h, 'pchip');
end

function [h, m] = preprocessing(H, M)
ha = sort(H) ; ma = sort(M) ; [m, t_] = unique(ma) ; h = ha(t_);
end
```

Appendix A.3. Clustering

The proposed identification method returns a model with a very high number of cells. In order to use the model, notably in computational electromagnetics softwares [28], it is mandatory to reduce the number of cells. The function `clusterCells` listed hereafter implements a simple clustering algorithm based on the k-means algorithm [33]. The algorithm requires as input arguments the original cells (`omega`, `kappa`) and the target number of clustered cells (`nb`) and returns the simplified model (`omega_c`, `kappa_c`). It must be noticed that the result of this function is not deterministic, due to the intrinsic randomness of the k-means algorithm.

```
function [omega_c, kappa_c] = clusterCells (omega, kappa, nb)
[ind, kappa_c] = kmeans(kappa, nb);
omega_c = zeros(size(kappa_c));
for n = 1 : nb
  omega_c(n) = sum(omega(ind==n));
end
[kappa_c, ind] = sort(kappa_c) ; omega_c = omega_c(ind);
end
```

References

[1] L. Dupre, J. Melkebeek, Electromagnetic hysteresis modelling: From material science to finite element analysis of devices, Int. Compumag Soc. Newsletter 10 (3) (2003) 4–15.

[2] E. Cardelli, Chapter 4 - advances in magnetic hysteresis modeling, Vol. 24 of Handbook of Magnetic Materials, Elsevier, 2015, pp. 323–409. doi:10.1016/bs.hmm.2015.10.002.

[3] S. Quondam Antonio, A. Faba, H. P. Rimal, E. Cardelli, On the Analysis of the Dynamic Energy Losses in NGO Electrical Steels Under Non-Sinusoidal Polarization Waveforms, IEEE Transactions on Magnetics 56 (4) (2020) 1–15. doi:10.1109/TMAG.2019.2959213.

[4] A. Fouineau, B. Lefebvre, a. pereira, F. Sixdenier, M.-A. Raulet, N. Burais, Development of a magnetic circuit component to predict magnetic waveforms and core losses in a circuit type software, in: EPE'17 ECCE Europe, Warsaw, Poland, 2017. doi:10.23919/EPE17ECCEEurope.2017.8098941.

[5] F. Sixdenier, M. A. Raulet, Current Sensor Modeling With A FE-Tuned MEC: Parameters Identification Protocol, IEEE Sensors Journal 12 (5) (2012) 859–863. doi:10.1109/JSEN.2011.2165841.

[6] E. Cardelli, A. Faba, M. Pompei, S. Quondam Antonio, Magnetic losses in Si-Fe alloys for avionic applications, AIP Advances 7 (5) (2017) 056112. doi:10.1063/1.4978456.

[7] F. Preisach, über die magnetische Nachwirkung, Zeitschrift für Physik 94 (5-6) (1935) 277–302. doi:10.1007/BF01349418.

[8] Mathematical Models of Hysteresis and Their Applications, Elsevier, 2003. doi:10.1016/B978-0-12-480873-7.X5000-2.

[9] A. A. Adly, I. D. Mayergoyz, A new vector Preisach-type model of hysteresis, Journal of Applied Physics 73 (10) (1993) 5824–5826. doi:10.1063/1.353539.

[10] E. Dlala, A. Belahcen, K. A. Fonteyn, M. Belkasim, Improving Loss Properties of the Mayergoyz Vector Hysteresis Model, IEEE Transactions on Magnetics 46 (3) (2010) 918–924. doi:10.1109/TMAG.2009.2034846.

[11] L. Zhu, W. Wu, X. Xu, Y. Guo, W. Li, K. Lu, C.-S. Koh, An Improved Anisotropic Vector Preisach Hysteresis Model Taking Account of Rotating Magnetic Fields, IEEE Transactions on Magnetics 55 (6) (2019) 1–4. doi:10.1109/TMAG.2019.2899592.

[12] E. Della Torre, E. Pinzaglia, E. Cardelli, Vector modeling—Part I: Generalized hysteresis model, Physica B: Condensed Matter 372 (1-2) (2006) 111–114. doi:10.1016/j.physb.2005.10.028.

[13] E. Della Torre, E. Pinzaglia, E. Cardelli, Vector modeling—Part II: Ellipsoidal vector hysteresis model. Numerical application to a 2D case, Physica B: Condensed Matter 372 (1-2) (2006) 115–119. doi:10.1016/j.physb.2005.10.029.

[14] E. Cardelli, E. Della Torre, A. Faba, Numerical Implementation of the DPC Model, IEEE Transactions on Magnetics 45 (3) (2009) 1186–1189. doi:10.1109/TMAG.2009.2012549.

[15] E. Cardelli, E. Della Torre, A. Faba, A General Vector Hysteresis Operator: Extension to the 3-D Case, IEEE Transactions on Magnetics 46 (12) (2010) 3990–4000. doi:10.1109/TMAG.2010.2072933.

[16] E. Cardelli, A General Hysteresis Operator for the Modeling of Vector Fields, IEEE Transactions on Magnetics 47 (8) (2011) 2056–2067. doi:10.1109/TMAG.2011.2126589.

[17] D. Jiles, D. Atherton, Theory of ferromagnetic hysteresis, Journal of Magnetism and Magnetic Materials 61 (1986) 48–60.

[18] A. Bergqvist, A simple vector generalization of the Jiles-Atherton model of hysteresis, IEEE Transactions on Magnetics 32 (5) (Sept./1996) 4213–4215. doi:10.1109/20.539337.

[19] J. Gyselinck, P. Dular, N. Sadowski, J. Leite, J. Bastos, Incorporation of a Jiles-Atherton vector hysteresis model in 2D FE magnetic field computations: Application of the Newton-Raphson method, COMPEL - The international journal for computation and mathematics in electrical and electronic engineering 23 (3) (2004) 685–693. doi:10.1108/03321640410540601.

[20] C. Guérin, K. Jacques, R. V. Sabariego, P. Dular, C. Geuzaine, J. Gyselinck, Using a Jiles-Atherton vector hysteresis model for isotropic magnetic materials with the finite element method, Newton-Raphson method, and relaxation procedure: Using a vector Jiles-Atherton hysteresis model, International Journal of Numerical Modelling: Electronic Networks, Devices and Fields 30 (5) (2017) e2189. doi:10.1002/jnm.2189.

[21] K. H. Carpenter, A Differential Equation Approach to Minor Loops in the Jiles-Atherton Hvsteresis Model, IEEE Transaction on magnetics 27 (6) (1991) 4404–4406.

[22] A. Bergqvist, Magnetic vector hysteresis model with dry friction-like pinning, Physica B: Condensed Matter 233 (4) (1997) 342–347. doi:10.1016/S0921-4526(97)00319-0.

[23] F. Henrotte, A. Nicolet, K. Hameyer, An energy-based vector hysteresis model for ferromagnetic materials, COMPEL International Journal of Computations and Mathematics in Electrical and Electronic Engineering 25 (1) (2006) 71–80.

[24] V. François-Lavet, F. Henrotte, L. Stainier, L. Noels, C. Geuzaine, An Energy-Based Variational Model of Ferromagnetic Hysteresis for Finite Element Computations, IEEE Transactions on Magnetics 49 (5) (May 2013).

[25] F. Sixdenier, R. Scorretti, Numerical model of static hysteresis taking into account temperature: Static hysteresis taking into account temperature, International Journal of Numerical Modelling: Electronic Networks, Devices and Fields 31 (2) (2018) e2221. doi:10.1002/jnm.2221.

[26] F. Henrotte, S. Steentjes, K. Hameyer, C. Geuzaine, Iron Loss Calculation in Steel Laminations at High Frequencies, IEEE Transactions on Magnetics 50 (2) (2014) 333–336. doi:10.1109/TMAG.2013.2282830.

[27] K. Jacques, S. Steentjes, F. Henrotte, C. Geuzaine, K. Hameyer, Representation of microstructural features and magnetic anisotropy of electri-

cal steels in an energy-based vector hysteresis model, AIP Advances 8 (4) (2018) 047602. doi:10.1063/1.4994199.

[28] M. R. Longhitano, F. Sixdenier, R. Scorretti, L. Krähenbühl, C. Geuzaine, Temperature-dependent hysteresis model for soft magnetic materials, COMPEL - The international journal for computation and mathematics in electrical and electronic engineering 38 (5) (2019) 1595–1613. doi:10.1108/COMPEL-12-2018-0535.

[29] O. Bottuscio, M. Chiampi, C. Ragusa, L. Rege, M. Repetto, Description of TEAM Problem: 32 A Test-Case for Validation of Magnetic Field Analysis with Vector Hysteresis.

[30] E. Cardelli, A. Faba, A. Laudani, S. Quondam Antonio, F. Riganti Fulginei, A. Salvini, A moving approach for the Vector Hysteron Model, Physica B: Condensed Matter 486 (2016) 92–96. doi:10.1016/j.physb.2015.12.001.

[31] E. Cardelli, A. Faba, F. Tissi, Surface field measurements in vector characterization of Si-Fe magnetic steel samples, International Journal of Applied Electromagnetics and Mechanics 44 (3-4) (2014) 331–338. doi:10.3233/JAE-141795.

[32] A. Quarteroni, F. Saleri, P. Gervasio, Scientific Computing with MATLAB and Octave (Fourth Edition), Springer-Verlag, BerlinHeidelberg, 2014.

[33] J. Macqueen, Some methods for classification and analysis of multivariate observations, in: Fifth Berkeley Symposium on Mathematical Statistics and Probability, Vol. 1, 1967, pp. 281–297.